RESEARCH ARTICLE

Macromolecular Materials and Engineering
Open Access
www.mame-journal.de

Development of Ductile-Sticky Bone Fillers from Biodegradable Hydrolyzed Wool-Keratin and Silk Fibroin

*Serife Bekar, Tugba Sezgin Arslan, and Yavuz Emre Arslan**

In the present study, a method is proposed for preparing novel ductile-sticky materials that can be used as bone void fillers using hydrolyzed wool-keratin (WK) and silk fibroin (SF). This methodology uses citric acid as a cross-linking agent in preparing keratin paste (KP) owing to its non-toxicity and plasticizing properties. The Keratin paste-silk fibroin structure (KPSF) is obtained by adding SF, which possesses biocompatible and superior mechanical properties. Methanol treatment is employed on the KPSF mixture to convert the Silk I structure in the SF to Silk II, resulting in a water-insoluble and tightly packed proteinaceous structure. The physicochemical properties of both bioscaffolds are investigated and discussed in detail by comparison. Based on the findings, the presence of SF in the KPSF structure contributed to properties such as flexibility and porosity. In ovo CAM analysis reveals that both materials exhibit proangiogenic properties and are biocompatible. KP and KPSF bioscaffolds can be converted into ductile-sticky forms by adding water. It believes that these forms can easily apply to bone defect areas, particularly cavitary bone defects. Furthermore, KPSF bioscaffolds, with better mechanical properties, can be considered candidates for use in non-load-bearing bone tissue engineering applications.

1. Introduction

Bone tissue, responsible for maintaining mineral storage, homeostasis, and blood pH, is a form of connective tissue that imparts mechanical support and flexibility to the body. This highly dynamic and vascularized tissue is a supportive element in the organism, attributed to its extracellular matrix (ECM) structure comprising organic (primarily made up of collagen type I) and inorganic components (e.g., hydroxyapatite).[1] Remodeling capacity, defined as continuous destruction and construction activities regarding the intimate crosstalk between osteoclasts and osteoblasts in the bone tissue, offers the opportunity to self-heal upon the damage, such as fractures or minor defects. However, bone's natural ability to renew itself remains inadequate for repairing the significant bone defects resulting from tumor resection, congenital malformation, trauma, fractures, and diseases such as osteoporosis or arthritis, and so necessitate surgical intervention.[2] Utilizing bone grafts is among the frequently employed surgical techniques to enhance bone regeneration in orthopedic procedures.[3] Worldwide, more than two million procedures for bone grafting are conducted annually to repair bone defects using bone autografts, allografts, or synthetic bone substitutes.[3,4] Even so, these strategies have some limitations, such as requiring a second surgical procedure, donor site morbidity, and risk of disease transmission. Hence, different tissue engineering strategies using natural and synthetic biomaterials have been studied to circumvent these limitations and increase bone regeneration capacity. Compared to synthetic biopolymers, there has been much attention on using natural ones for bone replacement due to their superior mimicry of ECM, biocompatibility, biodegradability, and versatility.[5,6] Also, they can be used in combination to support suitable mechanical durability.[6] Animal or plant-sourced polymers can be classified as proteins, polysaccharides, and polynucleotides. Prominent instances of common proteins used for tissue engineering include collagen, silk fibroin, albumin, elastin, keratin, and specially engineered polypeptides designed for specific functions.[5] Among them, keratin-based materials have been widely used in different forms, such as sponges, films, and hydrogels, in many biomedical applications owing to their natural abundance, biodegradability, and enhanced cell-material interactions.[7,8] Moreover, since keratin is regenerated from keratinous waste materials such as hair, wool, nails, and feathers, substantial quantities of this protein can be produced without animal sacrifice, unlike other osteoconductive proteins of animal origin.[8] Silk fibroin (SF) is another natural protein with a unique β-sheet-rich structure. It has received significant attention in bone regeneration applications thanks to

S. Bekar, T. Sezgin Arslan, Y. E. Arslan
Regenerative Biomaterials Laboratory
Department of Bioengineering
Faculty of Engineering
Çanakkale Onsekiz Mart University
Çanakkale 17100, Turkey
E-mail: emre.arslan@comu.edu.tr

The ORCID identification number(s) for the author(s) of this article can be found under https://doi.org/10.1002/mame.202400144

DOI: 10.1002/mame.202400144

its excellent biocompatibility, biodegradability, mechanical properties, and easy processing in different forms.[9,10] Whether of natural or synthetic biopolymer origin, an optimal bone substitute should possess multiple characteristics, including bioactivity, biocompatibility, biodegradability, osteoconductivity and/or osteoinductivity, adequate mechanical resistance for loading and weight-bearing, an interconnected porosity for delivering nutrients and oxygen to surrounding cells.[11,12] In this sense, chemically modifying biopolymers is often necessary to obtain next-generation biomaterials with the tailored substantial properties mentioned above. Various crosslinking reactions between functional groups within the repeat units (e.g., amines, hydroxyl groups, carboxylic acids) of biopolymers, especially proteins, are used to carry out these modifications. Thus, combining organic and/or inorganic moieties with different properties into a single hybrid structure to create biopolymeric networks tailored to possess the desired characteristics for specific applications is possible. The resulting bioscaffolds mechanical strength and porosity properties depend on the crosslinking degree, method, biopolymer concentration, and components.[13] With the inspiration of native ECM, various techniques were applied in our previous studies for developing bone material in different forms, including porous bioscaffolds,[14,15] cryogels,[16,17] and electrospun fiber,[18] which had promising results. However, when it comes to cavitary bone defects, which are challenging to reach, one of the most valuable issues for surgery is fabricating innovative biomaterials with intraoperative mouldability and appropriate use properties. In that context, injectable (as liquid or as a paste) bone substitutes with degradable properties are intensely studied to ensure convenient handling characteristics.[12,19] Among these, bone cement stands out as a promising candidate for clinical use in orthopedic trauma surgery, owing to its favorable properties regarding bioactivity, osteoconductivity, injectability, and moldability.[4,20,21] In a study by De Guzman and co-workers,[22] a keratose biomaterial, the oxidized form of hair filament proteins via peracetic acid, was developed and evaluated its effectiveness as a BMP-2 carrier system in bone tissue engineering applications. They also reported that these structures were effective in filling the bulk injury gap in segmental bone defects due to their malleability. Within this concept, this study presents a method to produce novel ductile-sticky like materials that can have potential use as bone void fillers. Citric acid, which acts as a crosslinker, plasticizer, and compatibilizer was used to obtain keratin-based paste (KP). A solution of silk fibroin (SF) was thoroughly mixed with the KP, resulting in the formation of the keratin paste-silk fibroin (KP-SF) structure. To obtain the uniform integration of the KP-SF structure, methanol treatment, which converted water-soluble silk I to water-insoluble silk II structures (antiparallel β-sheet crystal), was performed. After KP and KPSF were molded in ductile-sticky form, they were lyophilized to obtain porous bioscaffolds. Structure and mechanical specifications were assessed for the KP and KPSF bioscaffolds comparatively. Furthermore, angiogenic potential and biocompatibility were investigated by in ovo chick chorioallantoic membrane (CAM) assay. To our knowledge, no bone-filling material in the literature has been obtained in a ductile and sticky form comprising WK, SF, and/or other natural polymers thus far.

2. Experimental Section

2.1. Materials

Raw wool samples were supplied by local wool manufacturers in Çanakkale, Türkiye. Raw B. mori silk cocoons were purchased from Koza Han, Bursa, Türkiye. Sodium hydroxide (NaOH, 98–100.5%, pellets), sodium sulfite (Na_2SO_3, anhydrous), sodium carbonate (Na_2CO_3), lithium bromide (LiBr), citric acid monohydrate ($C_6H_8O_7.H_2O$), methanol (≥99.5%, MetOH), bovine serum albumin (≥ 96%, lyophilized powder), sodium azide (≥99.5%, NaN_3), proteinase K from Tritirachium (≥30 units/mg protein, lyophilized powder), 5,5-dithio-bis-(2-nitrobenzoic acid) (DTNB (Ellman's Reagent), glutaraldehyde (25% in H_2O) and formaldehyde (≥36.0% in H_2O) were purchased from Merck (Germany).

2.2. Extraction of Wool Keratin (WK)

A sulfitolysis reaction was performed by following the instructions stated in our previous study to obtain wool keratin.[16] Briefly, clean, and defatted wool fibers (5 g) were chopped into snippets and immersed in an extraction solution (100 mL) containing NaOH (5%, v/v) and Na_2SO_3 (5%, w/v). The mixture was then incubated in a bench-top shaker incubator (Benchmark Scientific, Incu-Shaker Mini, USA) set at 40–50 °C until no insoluble parts remained for ≈2 h. After purification steps, including filtration, centrifugation, and dialysis, the resulting extract was lyophilized. Hydrolyzed wool-keratin (WK) powder was stored at −26 °C for further experiments (**Figure 1A**).

2.3. Regeneration of Silk Fibroin (SF)

Pure silk fibroin (SF) protein was extracted from Bombyx mori silkworm following a previously reported protocol with a moderate modification.[23] Silk cocoons were cut into four equal parts using scissors, and silkworms were disposed of. For degumming processing, where the glue-like sericin protein was removed, cocoon pieces were treated with a boiling aqueous solution of 0.02 M sodium carbonate for 15 min. Meanwhile, it was stirred with a spatula occasionally to obtain a good dispersion of silk cocoons. The whole content was rinsed with ultrapure water (Milli-Q water) three times and dried in a fume hood. An aqueous silk fibroin solution was prepared by dissolving the degummed silk (1 g) in 9.3 M LiBr solution (4 mL) for 2 h in a water bath (Rotavapor R-210, Buchi, Flawil Switzerland) set at 60 °C. To remove excessive LiBr, the resulting silk fibroin solution, which was in color amber, transparent, and highly viscous, was dialyzed against ultra-pure water (Milli-Q water) using a cellulose tubing membrane (MWCO:14000 Da, Merck) for 72 h by changing the water daily. The dialysate was then centrifuged for 20 min at 9600 rpm (Hettich, MIKRO 120, Germany) to remove impurities and insoluble parts. After the purification processes, a colorless and optically clear silk fibroin solution was obtained and stored at 4 °C for further analysis and reactions (Figure 1B).

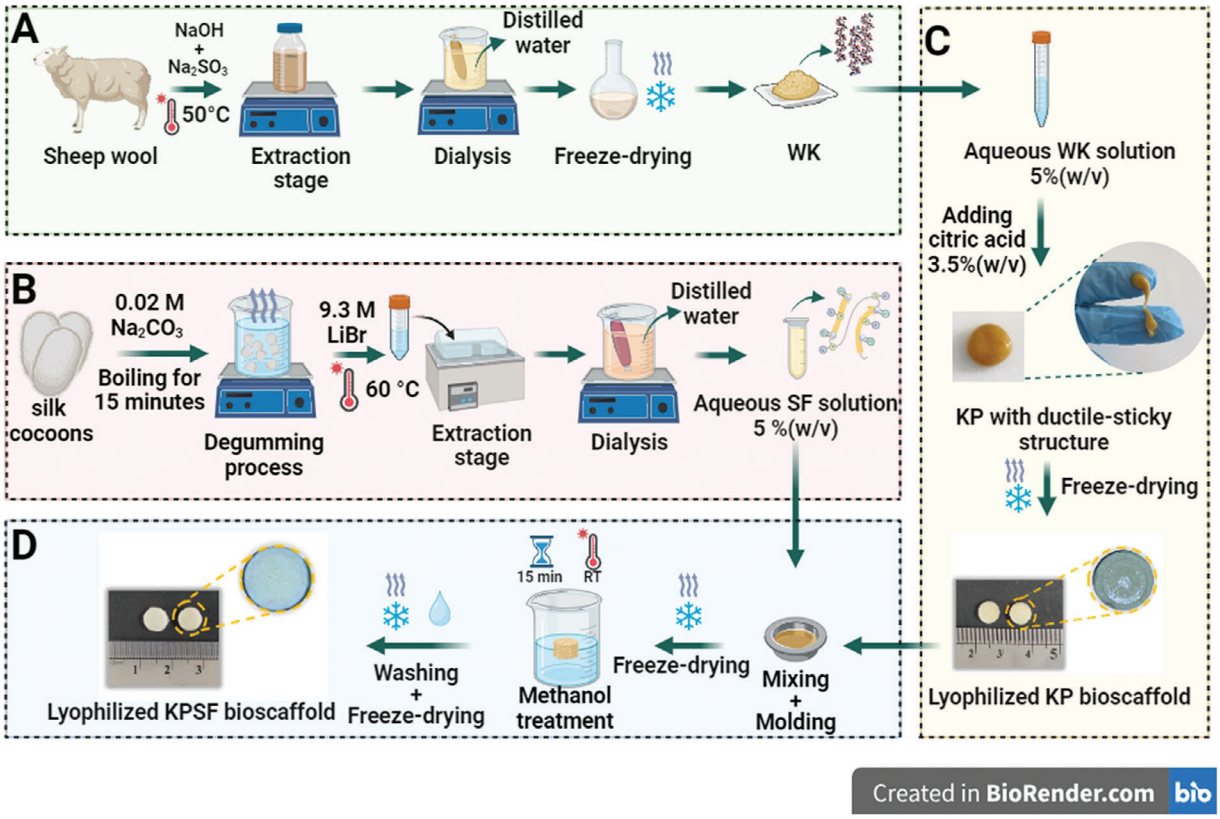

Figure 1. Schematic representation of the proposed methodology: WK extraction and purification process A); overall process for the SF dissolution B); preparation of KP C) and KPSF D) bioscaffolds.

2.4. Biochemical Characterization of Regenerated SF and WK Extracts

The protein content of the WK dialysate was determined by Lowry protein assay. The final concentration of the SF aqueous solution was determined by weighing the solid mass after the lyophilization of the silk solution with a specific volume. Additionally, the molecular mass range of the regenerated SF solution, and bovine serum albumin (BSA) as a negative control was determined using Sodium Dodecyl Sulfate-Polyacrylamide Gel Electrophoresis (SDS-PAGE) with the Laemmli method, employing a 12.5% resolving gel and a 4% stacking gel. The amounts of proteins loaded onto the gel per well were 0.5 µg and 125 µg for BSA and SF, respectively. A routine Colloidal Coomassie Blue (CCB, G-250) staining procedure was applied to make the protein bands in the gel visible. The free thiol (—SH) content in the WK was also determined by Ellman's assay using the standard calibration curve obtained from external standards of L-cysteine. Equation (1) given below was used to calculate the amount of free —SH groups:

$$Free\ SH\ Groups\ \frac{(mmol)}{Keratin\ (mg)} = \frac{\left[\left(\frac{OD412}{slope}\right) x\ (Dilution\ Factor\ x\ Total\ Volume)\right]}{Keratin\ Weight\ (mg)} \quad (1)$$

The analysis mentioned above and the necessary additional notes can be found in our previous studies.[14,16,24]

2.5. Construction of KP and KPSF Ductile-Sticky Void-Filling Materials

Keratin was dissolved in distilled water at a concentration of 5% (w/v). Subsequently, citric acid was gradually added to this solution under stirring conditions until the final concentration of citric acid in the solution reached ≈3.5% (w/v). Brown-colored keratin aggregates were formed when the solution pH was 4–4.2 with the addition of citric acid. These agglomerates were collected and washed with distilled water three times for 5 min to neutralize. The ductile-sticky keratin paste (KP) was molded and lyophilized to obtain a porous KP bioscaffold (Figure 1C). Lyophilized KP with a rigid structure was crushed into fine powder. 50 mg of powder KP was added into 150 µL of silk solution (5%, w/v); following this, the mixture was thoroughly kneaded by hand to obtain KPSF as a ductile-sticky and lyophilized overnight. The post-treatment process was made as in a previous study[25] to convert the amorphous SF in the structure into a β-sheet crystal structure to obtain water-insoluble, thermally, and mechanically durable KPSF material. For this purpose, the lyophilized KPSF bioscaffold was immersed in the methanol (>99.9% purity) for 15 min. After the washing and lyophilization process was repeated, a post-treated KPSF bioscaffold was obtained (Figure 1D). The

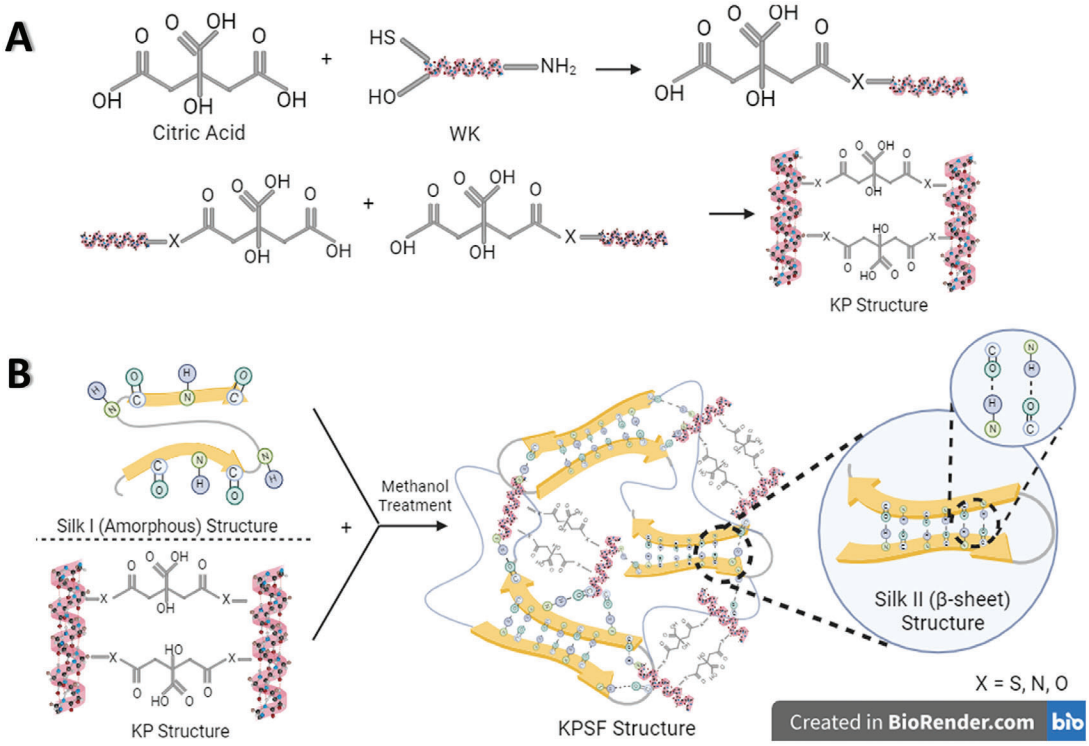

Figure 2. An overview of the mechanism of cross-linking. KP was obtained by the formation of new covalent bonds between citric acid and functional groups such as amine, hydroxyl, and sulfhydryl in keratin A). Treatment of the KPSF composite material with methanol leads to the conversion of Silk I in SF into Silk II, obtaining tightly packed proteinaceous structures B).

schematic representation of the crosslinking reactions occurring during the synthesis of KP and KPSF is presented in **Figure** 2A,B.

2.6. Physicochemical Analysis of KP and KPSF Materials

The structural changes of the KP and KPSF bioscaffolds were evaluated using the attenuated total reflectance Fourier transform infrared spectroscopy (ATR-FTIR) and X-ray diffraction (XRD) analysis (PANalytical Empyrean, Malvern Panalytical, Netherlands). The thermal behavior of the samples was also investigated using a thermogravimetric analyzer (TGA 8000, Perkin Elmer, USA). The microarchitecture and porous structure of the materials were investigated using field emission scanning electron microscopy (FE-SEM JFM 7100F EDS, JEOL, Japan). Detailed methods of the related analyses were presented in our previous study.[16]

A uniaxial compression test was applied to test the behavior of materials under applied crushing with a 200N load cell using a micromechanical testing device (Univert CellScale Biomaterials Testing, Canada). KP (cylindrical, ø = 3.9 mm; h = 3.5 mm) and KPSF (cylindrical, ø = 3.6 mm; h = 3.8 mm) materials were placed between the two plates and compressed at a rate of 0.025 mm s^{-1}. Meanwhile, a tripod camera (HD 1080p, Logitech) captured the real-time images at a frequency of 5 Hz. The samples compressive modulus was calculated as the initial and final slopes of the linear part of the stress–strain curve using the Origin Pro 8SR0 (v8.0724, Origin Lab Corporation, Northampton, MA, USA) software.

2.7. In Vitro Enzymatic Biodegradation Study

A proper balance between new tissue formation and resorption was crucial in organisms. Therefore, new-generation biomaterials that support regeneration must be capable of achieving this balance. In that context, in vitro biodegradation rates of the KP and KPSF bioscaffolds were determined by the enzymatic process described in our previous study.[16] According to this procedure, after the initial dry weights (m_i) of the samples were noted, they were immersed in Tris-HCI buffer (0.02 M, pH 8.0), including preservative (NaN_3, 0.05%, w/v) and proteinase K (0.01%, w/v). Samples were incubated in the enzyme solution at 37 °C for 3 and 10 days. After each time point, the samples were retrieved, washed, lyophilized, and reweighed (m_f: final weight). The degradation rate was calculated using the Equation (2) given below:

$$Weight\ Loss\ \ (\%) = \frac{(m_i) - (m_f)}{(m_f)} \times 100 \qquad (2)$$

2.8. In Ovo Chick Chorioallantoic Membrane (CAM) Assay and Characterizations

To evaluate the biocompatibility and angiogenic response of the KP and KPSF materials, a chicken in ovo cam assay was performed as in our previous studies.[26,27] Freshly fertilized chicken eggs were supplied from a local farm in Çanakkale, Türkiye. Following cleaning and disinfection, eggs were placed vertically in

the rotating tray inside an egg brooder (Brinsea Ovation 28 Advance Ex, U.K.) and incubated at 37.5 °C and 60% relative humidity (RH) while rotating every 120 min for 3 days. On the 3rd day of embryonic development (EDD3), small windows were cut from the sharp end of the eggs and stretched to close with a sterile parafilm on openings to prevent contamination or drying of the egg contents. Incubation of windowed eggs was maintained in the same conditions until material implantation. On EDD9, sterilized materials were carefully placed between prominent veins on the CAM surface and imaged using a stereo microscope (Stemi 305, Zeiss) with a digital camera (Axiocam 105 color, Zeiss). Four days after implantation (EDD 13), micro vessels following to the grafts were captured. The images were then analyzed using ImageJ 1.51j (National Institutes of Health, Bethesda, MD, USA) to measure vascular density within the 1 mm imaginary area surrounding the grafts. The angiogenic response was assessed using the vascular index, calculated as the ratio of vascular density at EDD13 to EDD9. After the imaging process, the experiment was terminated, and the materials were dissected with ≈1 cm of CAM around them. CAM-materials complexes were processed as in our previous study[26] for SEM and histological analyses (sectioning and routine hematoxylin and eosin staining). Chick embryos do not suffer pain during any application until the 15th day of their development and were not considered alive before the 17th of their development[28,29] Therefore, ethical approval was unnecessary as the in-ovo CAM analysis was completed within 13 days.

2.9. Statistical Analysis

The results were presented as mean ± standard deviation, and each experiment was conducted in triplicate for quantitative analysis. Statistical significance between groups in experimental sets was determined using one-way analysis of variance (ANOVA) with Origin Pro 8 SR0 software (v8.0724, Origin Lab Corporation, USA), followed by Tukey's test. Experimental groups were considered to have a statistically significant difference if the p-value was < 0.05 obtained from the ANOVA test.

3. Results and Discussion

3.1. Biochemical Assessments of WK and SF Extracts

Biochemical characterization of human hair keratin extracted by sulfitolysis reaction was carried out in-depth in our previous study.[16] In the current study, wool, which is very similar to the structure of hair, was used as the raw material, and other necessary processes were applied precisely. Keratin content in the dialysate was found to be 8.31 ± 0.46 mg mL^{-1} using the calibration curve obtained by the modified Lowry assay (**Figure 3A**). Additionally, the yield based on dry weight was 40.52 ± 0.16%. Keratin differs from other structural proteins due to its extensive cysteine linkage. During WK extraction with the sulphitolysis reaction, disulfide bonds in cysteine residues of the keratin are broken to give cysteine thiol (cysteine-SH) and S-sulfonated residue structures. Therefore, the amount of -SH sulfhydryl groups reflecting the cysteine residues in WK extracts was quantitatively determined by Ellman's analysis using the L-cysteine calibration curve (Figure 3B) and Equation (1), yielding 0.0682 ± 0.011 mmol SH/mg keratin. The findings regarding the analysis of protein content and free-SH group quantities are consistent with our previous study.[16] Furthermore, in our previous study,[16] SDS-PAGE and matrix-assisted laser desorption/ionization-time of flight (MALDI-TOF) mass spectrometry (MS) analysis was conducted to determine the molecular weight (MW) profile of keratin polypeptide chains extracted through the sulphitolysis reaction. The SDS-PAGE pattern of the keratin extract showed a band at ≈6–8 kDa. In order to determine the MW distribution of the keratin extract more accurately, MALDI-TOF MS analysis was performed within the mass range of 0–10,000 Da according to the findings (6–8 kDa) obtained from the SDS-PAGE. Based on the MALDI-TOF MS spectrum obtained previously, we stated that hydrolyzed keratin was obtained in small fractions with a Mw of ≈2–3 kDa, as the polypeptide backbone of keratin was disrupted during the extraction process in an alkaline environment. Small fractions of keratin can provide more active functional groups that can react with other natural and synthetic polymers. This is important for synthesizing new-generation materials used in tissue engineering applications. In addition, the proposed method can offer other advantages, such as being non-toxic, cheap, and having a short reaction time.[16]

The concentration of the regenerated SF solution was determined to be 6.8–7% (w/v) using the gravimetric method, which involved weighing freeze-dried samples of a known volume of the SF solution. In studies[23,30] where extraction protocol with LiBr was used to dissolve the SF, the concentration was obtained as 7–8% (w/v), similar to our findings.

Figure 3C shows the SDS-PAGE pattern of the regenerated SF solution. From the electrophoretic profile of the SF, a very broad band in the range of 50–350 kDa corresponds to the peptides derived from the degradation of the heavy chains of fibroin, while a distinct band at ≈24 kDa represents the light chains.[31] The broad smear band above 250 kDa was formed due to the serious damage to the peptide chains of silk fibroin caused by the Na_2CO_3 used during degumming.[32,33]

3.2. Physico-Chemical Evaluations Lyophilized KP and KPSF Scaffolds

ATR-FTIR spectroscopy was utilized to detect functional groups of production materials and characterize chemical bonding. **Figure 4A** shows the FT-IR spectra of the WK, SF, KP, and KPSF materials. Vibrations due to the four characteristic bands of proteins are seen in all spectra. The Amide A broad band between 3200–3400 cm^{-1} corresponds to the H-bonded N—H stretching vibration. The amide I, II, and III bands that elucidate the conformational structures of proteins and polypeptides are also seen. The amide I band at 1600–1700 cm^{-1} and the amide II band at 1500–1600 cm^{-1} are related to the C═O stretching and N—H deformation with some contributions of C—N stretching, respectively. The amide III band at 1200–1300 cm^{-1} belongs to C—N and C—C stretching absorptions and N—H and C—O bending absorptions.[16,34] Compared to the WK spectrum, the KP spectrum has a small shoulder peak at ≈1740 cm^{-1}, assigned to the C═O stretching modes of citric acid, indicating that

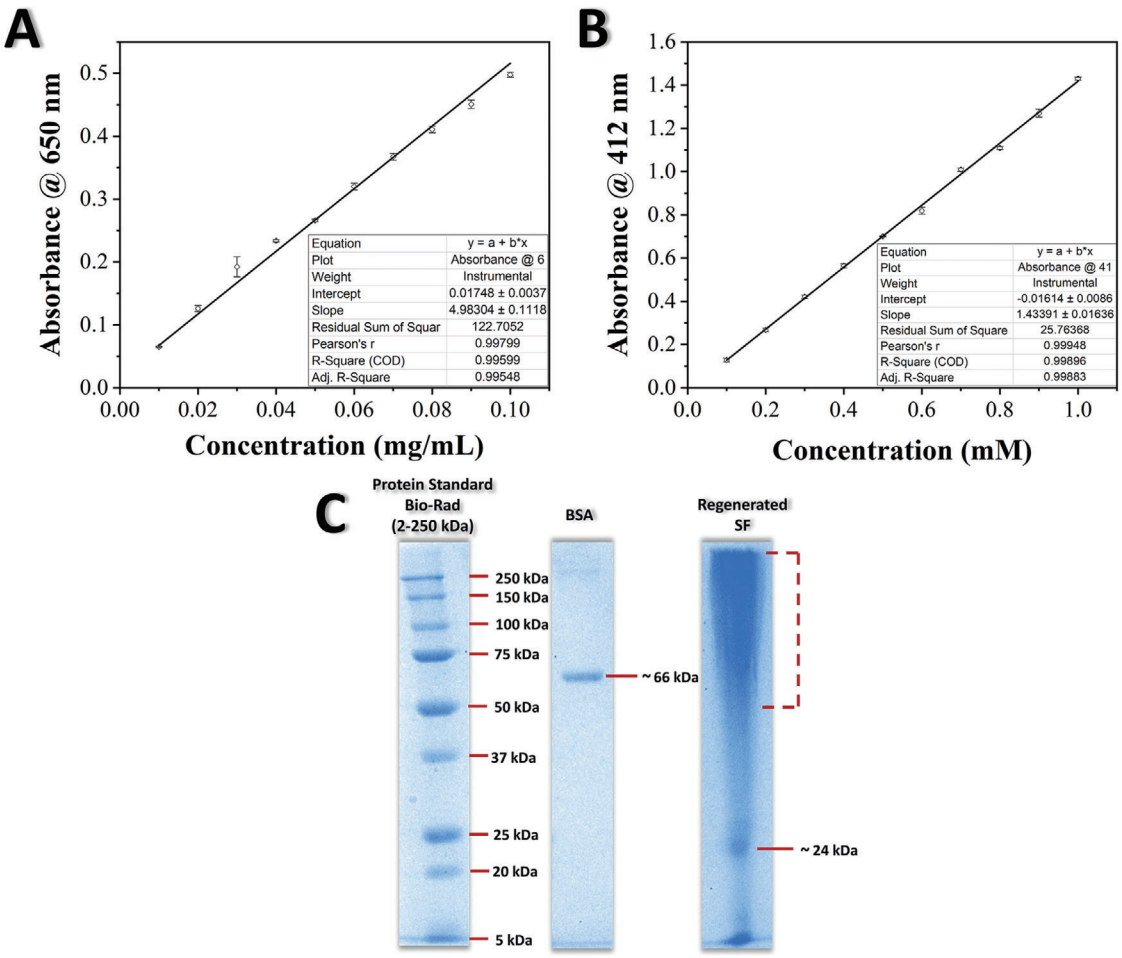

Figure 3. Standard calibration curves were obtained with Lowry's Assay A) and Ellman's Assay B) to calculate the protein content and free -SH groups of hydrolyzed WK, respectively. The SDS-PAGE pattern of regenerated SF C).

cross-linking reactions between citric acid and keratin have been achieved.[34] On the other hand, citric acid, with multi-carboxylic groups, forms strong hydrogen bonds with the hydroxyl and amine groups in the protein structures.[35,36] Therefore, the intensity differences in the amide peaks of WK and KP may be attributed to the formation of hydrogen bonds. Silk fibroin can be in a water-soluble amorphous (Silk I) and a water-insoluble crystalline conformation (Silk II). Silk I represents an intermediate state between α-helix and β-sheet, while Silk II represents an anti-parallel β-sheet structure and is more stable than Silk I. The amide peaks observed in the SF spectrum correspond to alpha-helix and β sheet structures. However, it can be said that SF consists mainly of Silk II, as its lyophilized form is insoluble in water. Moreover, a decrease in the intensity of the amide peaks is observed in the KPSF spectrum compared to the SF, indicating the β-sheet structures decrease by incorporating KP containing more α-helix to the SF.[37]

Structural changes and the crystal phase of the samples were also determined using XRD analysis; the obtained spectra are shown in Figure 4B. The diffraction peak ≈20° was related to the anti-parallel β-sheet structure in the WK structure. On the other hand, the XRD pattern of the WK does not exhibit the peak ≈2θ = 9° corresponding to the α-helix structure in natural wool, as the α-helix is disrupted by an alkaline treatment during the sulphitolysis reaction.[38] The newly appeared peak ≈2θ = 9° in the KP spectrum indicates that the alpha-helix structure was re-established after crosslinking with citric acid. This can be attributed to the formation of strong hydrogen bonds between the carboxyl groups of citric acid and the —OH groups of the wool keratin structure to trigger conformational changes.[35] The appearance of a peak in the SF spectrum confirmed the β-sheet structure in the Silk II crystalline conformation.[39] The presence of two significant peaks ≈2θ = 9° and 20° in the spectrum of KPSF, corresponding to the α-helix and β-sheet structures, along with a slight increase in their intensity due to the overlapping of peaks in the same region, can provide evidence for the successful preparation of the composite. Another explanation of why KPSF gave a similar spectrum to the KP can be the usage of many amounts of KP during the preparation of KPSF material.

Thermogravimetric curves of the samples depicting changes in weight by thermal degradation are given in Figure 4C. In all curves, the first stage of the weight losses observed below ≈100 °C indicates the evaporation of moisture. The second stage of weight loss in the temperature range of ≈300–600 °C is mainly attributed

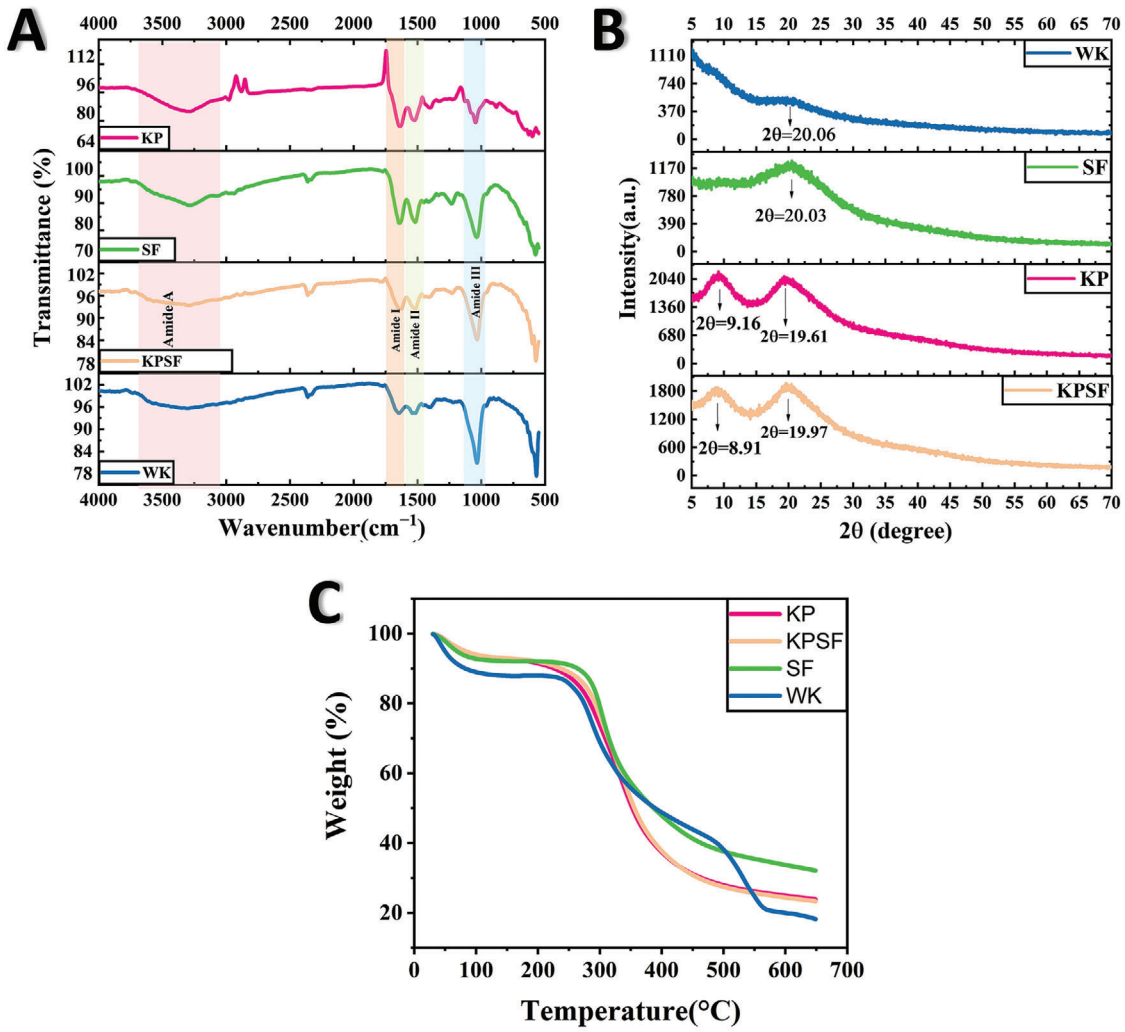

Figure 4. ATR-FTIR spectra A), XRD patterns B), and TGA curves of WK, SF, KP, and KPSF bioscaffolds C).

to the degradation of proteins.[40] At 600 °C, the weight losses for WK and SF are 80% and 60%, respectively. Additionally, KP and KPSF exhibited similar thermal degradation curves, with mass losses at 600 °C approximately reaching 70%. The reason KP exhibits better thermal stability than WK can be attributed to the formation of new covalent bonds between citric acid and functional groups such as amine, hydroxyl and sulfhydryl in keratin during a crosslinking reaction.[41] According to our findings, the natural biomaterial with the highest thermal stability is SF. Contrary to expectations, we observed that the inclusion of SF did not enhance the thermal stability of the KPSF material. This is because there is too much KP with less thermal stability than SF in the composite.

3.3. Investigation of Pore Sizes and Microarchitectures of Lyophilized KP and KPSF Bioscaffolds

SEM analysis was performed to investigate the morphology and pore arrangement of the materials. SEM micrographs at x250, x1000, and x2500 magnifications of KP and KPSF bioscaffolds are given in **Figure 5**. The formation of a porous structure in both materials was achieved using the lyophilization technique. Figure 5A shows that the KP bioscaffold had irregular pore shapes and sizes. In Figure 5B, the KP-SF scaffold exhibited homogeneous and interconnected 3D structures. In conclusion, the addition of pure SF with a β-sheet structure resulted in the formation of a well-interconnected porous structure through molecular interactions between the polypeptide chains of SF and KP.[37] In addition, the mean pore sizes of the KP and KPSF scaffolds were found to be 35.64 ± 20.93 and 45.76 ± 14.50 µm, respectively. A suitable biomaterial needs to be porous to allow the proliferation, migration, and differentiation of cells, as well as vascularization. In addition, porosity ensures the integration and mechanical stability between the biomaterial implanted in the damaged area and the surrounding natural tissue.[42] Even though optimum pore size depends on the used material type, application area, and strategy, a pore size range of 10–100 µm can be appropriate for bone engineering scaffolds in vitro.[43,44] In this context, micropores provide a larger surface area that

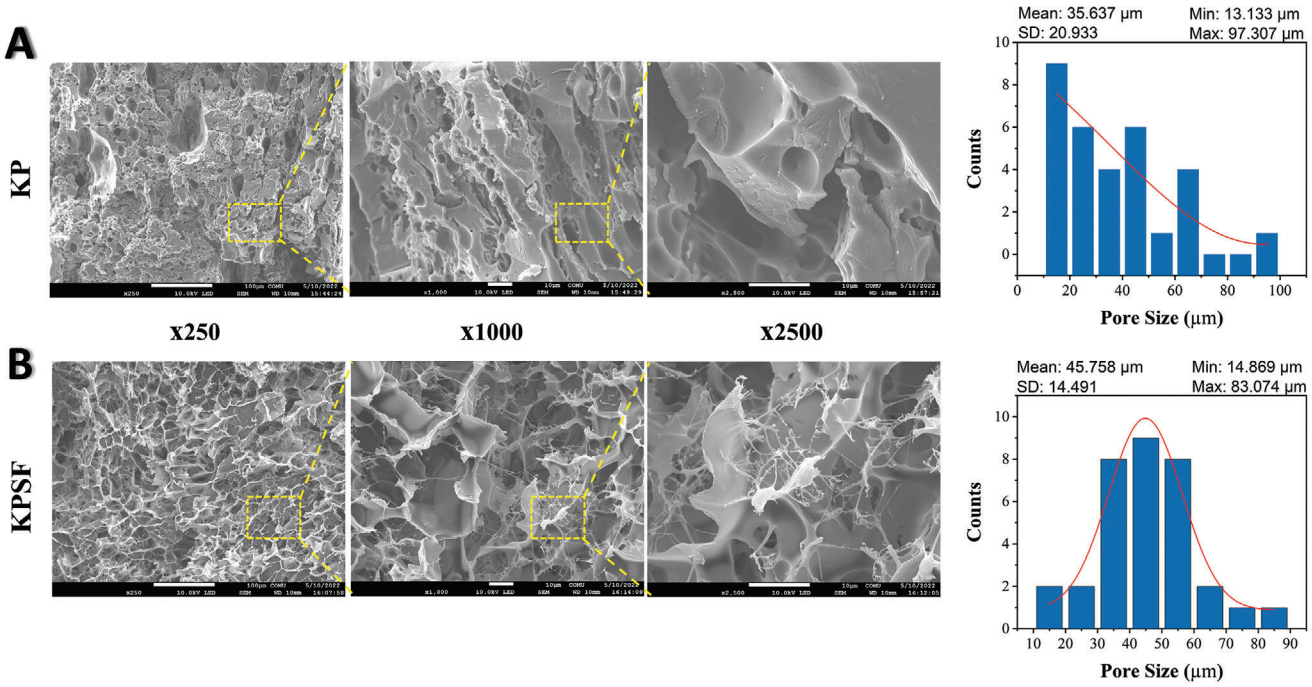

Figure 5. SEM micrographs of KP A) and KPSF bioscaffolds B) at x250, x1000, and x2500 magnifications with pore size distribution histograms.

facilitates ion exchange and bone protein adsorption, while macropores are beneficial in cell infiltration and differentiation events that occur during osteogenesis.[45] Based on our findings, KPSF would be a good candidate in bone tissue engineering applications as it offers the mentioned balance regarding pore size and interconnected network.

3.4. Assessment of Mechanical Durability of KP and KPSF Bioscaffolds

Compression tests were carried out to investigate the mechanical properties of KP and KPSF bioscaffolds in dry form, and real images were captured during the test (**Figure 6**). Compressive

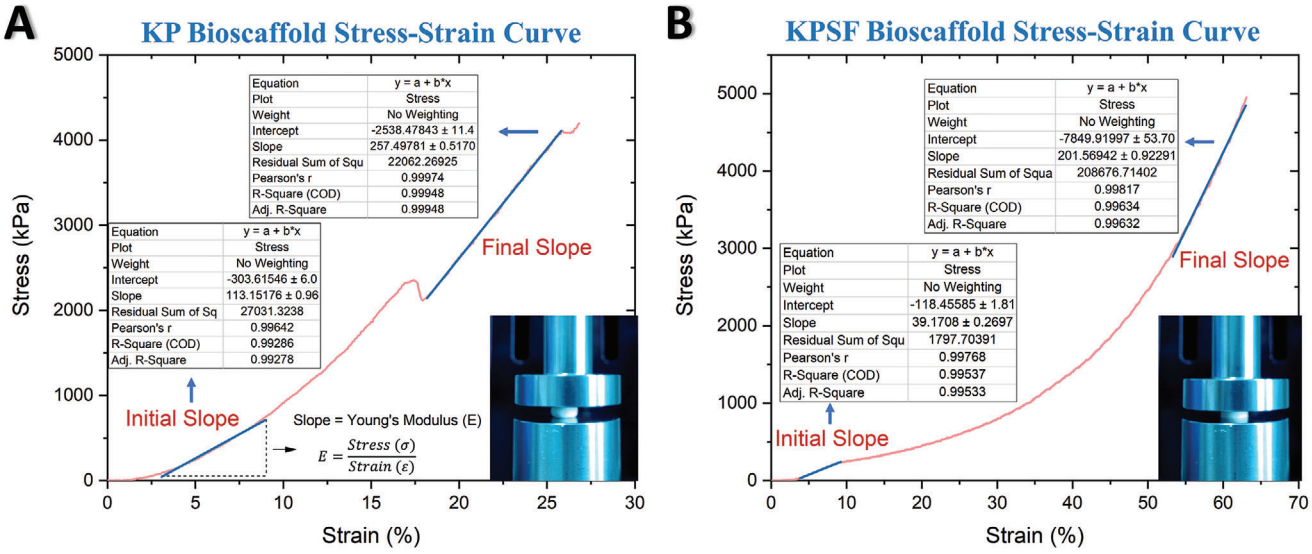

Figure 6. The Stress–Strain curves and compressive testing images of the KP A) and KPSF B) bioscaffolds.

Table 1. Compressive test results.

Sample	Compression Stress [MPa]	Compression Strain [%]	Young's Modulus [MPa]	
			Initial	Final
KP	4.193 ± 0.443	26.830 ± 1.877	11.32 ± 0.96	25.75 ± 0.52
KPSF	4.952 ± 0.102	63.068 ± 2.056	3.92 ± 0.27	20.16 ± 0.92

stress and Young's modulus values were summarized in **Table 1**. The ultimate compressive stress of the KP and KPSF bioscaffolds were found to be 4.193 ± 0.443 MPa and 4.952 ± 0.102 MPa, while the strain (%) values were observed as 26.830 ± 1.877% and 63.068 ± 2.056%, respectively. The Young's modulus of the KP and KPSF bioscaffolds was computed from the initial and final slope values of the linear regions of the stress–strain curves in Figure 6A,B. MaximumYoung's modulus values of KP and KPSF bioscaffolds were found as 25.75 ± 0.52 MPa and 20.16 ± 0.92 MPa, respectively. The mechanical compression tests indicated that KP, with a higher Young's modulus value, possesses a more rigid structure and exhibits greater resistance to deformation and stretching under exposure to force in comparison to the KPSF scaffold. This result also explains why KP shows a lower strain value when subjected to a given stress. Moreover, the stress-strain curve of KP exhibits a minor fracture caused by the sudden release of stored energy when subjected to compressive stress (Figure 6A). In contrast, the stress–strain curve of the KPSF scaffold did not exhibit any failure under the compression test, suggesting its elastic structure (Figure 6B). While the influences of porosity and pore size on the mechanical properties of materials remain controversial in the literature, some studies have reported that porous materials, especially with larger pore sizes, lead to a decrease in stiffness.[46,47] Based on our findings, it can be concluded that incorporating SF resulted in a KPSF bioscaffold with a more porous and elastic structure. When compared with the literature, it was seen that KP and KPSF bioscaffolds had higher compressive strength and modulus in dry conditions than natural-based biomaterials containing keratin,[48,49] silk fibroin,[50] and silk fibroin/wool keratin.[37]

Moreover, owing to its robust and flexible structure, the lyophilized KPSF bioscaffold can be considered a candidate for use in non-load-bearing bone tissue engineering applications. After adding water to lyophilized KPSF and KP readily reverted to its original ductile-sticky form. You can see the wettability and moldability properties of KPSF and KP in Videos S1–S4 (Supporting Information), given in the supporting information file. The resulting moldable KP and KPSF materials can effectively fill cavitary bone defects and provide mechanical support.

Table 2. In vitro resorption rates of KP and KPSF bioscaffolds.

Sample	Biodegradability, Weight Loss [%]	
	Day 3	Day 10
KP	3.29 ± 1.09	7.44 ± 2.40
KPSF	8.82 ± 1.63	16.96 ± 0.78

3.5. Determination of In Vitro Resorption Rates of KP and KPSF Bioscaffolds

Tissue-engineered scaffolds should possess a proper biodegradation rate, which is essential for inducing the regeneration of diverse tissues or organs. To this end, the in vitro resorption rates of KP and KPSF bioscaffolds were determined by exposing the samples to the enzymatic solution for 3 and 10 days at 37 °C. At the end of the experimental sets, it was observed that the bioscaffolds incubated in the enzymatic solution retained their morphology and structural integrity, albeit with a slight softening in the aqueous solution. Resorption rates of the KP and KPSF bioscaffolds were calculated as a percentage of weight loss and given in **Table 2**. The total weight losses of KP and KPSF bioscaffolds were 3.29 ± 1.09% and 8.82 ± 1.63% on day 3, respectively. On the other hand, weight losses on day 10 for the same scaffolds were 7.44 ± 2.4% and 16.96 ± 0.78%. These results indicate minimal weight changes in both bioscaffolds for the incubation days 3 and 10. However, it was observed that the weight loss of KPSF increased about two times on both incubation days compared to KP, which can be attributed to KPSF being more porous than KP. Due to their high water uptake capacities, porous materials exhibit increased uptake rates of the enzyme solution used in the experiment, making the biomaterial more susceptible to proteolytic attacks and accelerating weight loss.[51]

3.6. In Ovo CAM Assay

CAM assay has been extensively used as an alternative to conventional animal models to assess the angiogenic potential and biocompatibility of the materials. Therefore, we performed in ovo cam assay and gained macroscopic, microscopic, and histological insights about the angiogenic potential and biocompatibility of our bioscaffolds (**Figure 7A–D**). Stereomicroscopic images of the lyophilized KP and KPSF bioscaffolds on the CAM surfaces at EDD9 and EDD13 revealed that their structural integrity was retained during the incubation (Figure 7A). The vascular index of the newly formed blood vessels within a specific area around the bioscaffolds was calculated using ImageJ software. From the binary images with a black-and-white scale, the blood vessel density indexes for KP and KPSF bioscaffolds were determined to be 1.13 ± 0.053 and 1.25 ± 0.057, respectively, with no statistically significant differences (Figure 7B, $p > 0.05$).

Hematoxylin and eosin staining were applied to view cellular and tissue structures in CAM-bioscaffold complexes. Figure 7C demonstrates that both bioscaffolds serve as favorable environments for cell infiltration and proliferation compared to the negative control groups. Additionally, the linkage regions represented by yellow arrows in the histological images provide evidence of

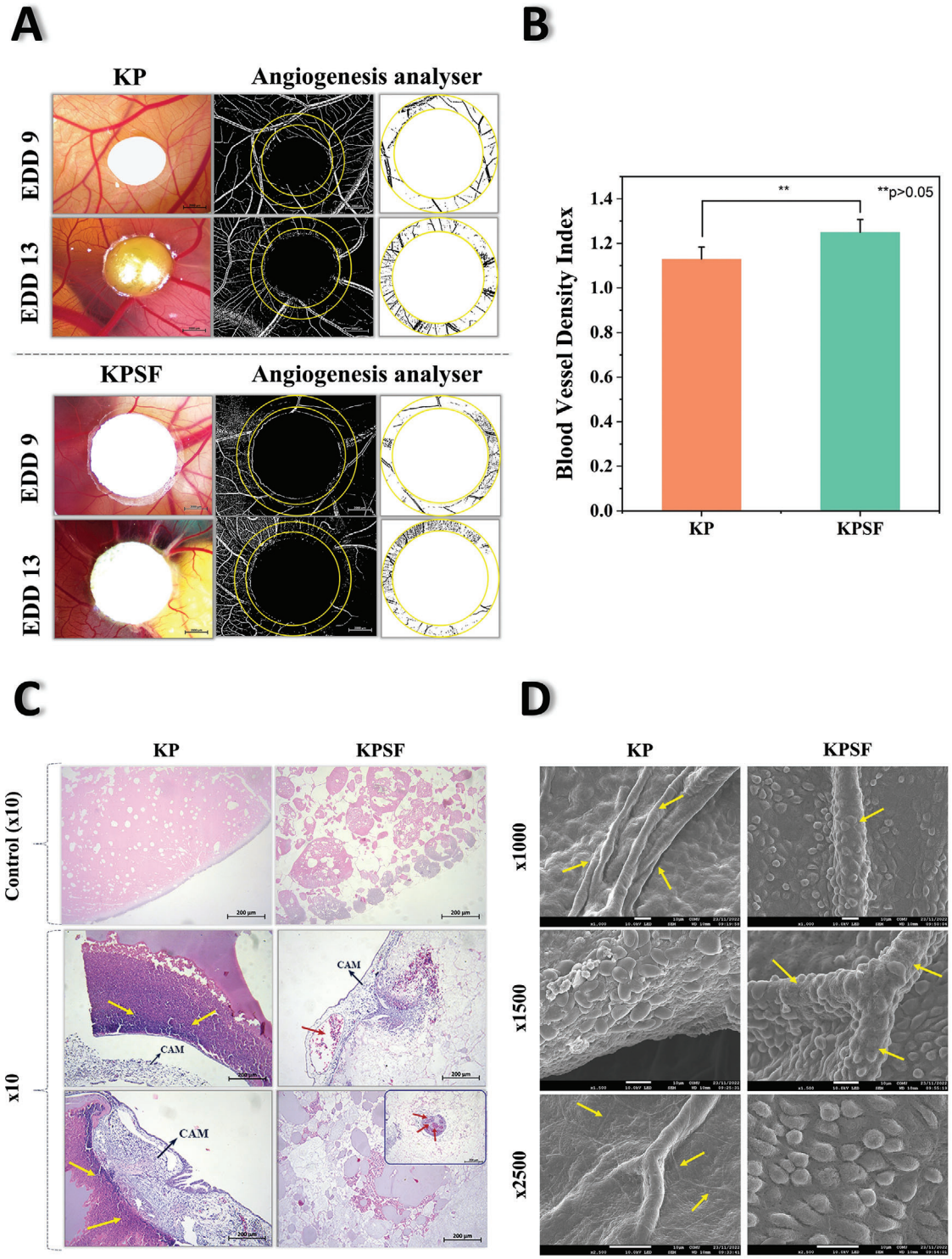

Figure 7. Assessment of biocompatibility and proangiogenic properties of KP and KPSF bioscaffolds. Stereomicroscopic and binary images of both bioscaffolds on CAM surface for EDD9 and EDD13 A). Blood vessel vascular index graph B). H&E staining of KP-CAM and KPSF-CAM complexes tissue sections at the EDD 10. Compared to the control groups, cell infiltration and proliferation were clearly seen on both bioscaffolds-CAM structures. In these histological images, red arrows indicate newly formed blood vessels, while yellow arrows indicate the linkage region between the CAM and the bioscaffold. Scale bars represent 200 µm (10X) C). SEM images at x1000, x1500, and x2500 magnifications. Yellow arrows indicate microvessel structures on the surface of bioscaffolds D).

cell invasion that fills the space between the CAM and bioscaffolds. The blood cells and vessels grooving toward the scaffolds were also observed. These results suggest that the scaffolds integrate effectively into the surrounding tissues. Furthermore, the bioscaffolds-CAM complexes did not cause adverse effects such as acute or chronic inflammation and necrosis, proving that both bioscaffolds were biocompatible.

Figure 7D shows SEM micrographs at magnifications x1000, x1500, and x2500 of the bioscaffolds-CAM tissue sections. Similar to histological evidence, blood cell adhesion, migration, proliferation, and microvascular networks were seen on the surfaces of both bioscaffolds.

4. Conclusion

This study introduces a novel pasty and moldable material prepared with wool keratin and silk fibroin. Citric acid has been utilized as a cross-linking agent in the preparation of KP owing to its non-toxicity, plasticizing, and stabilizing properties. A water-insoluble, mechanically and thermally durable, and ductile-sticky material was produced through cross-linking reactions between the three carboxylic acid groups in citric acid and functional groups such as —NH2, —SH, and —OH in WK. The easily shaped material was lyophilized to obtain a porous KP bioscaffold. Silk fibroin, possessing biocompatible and superior mechanical properties in liquid form, was mixed thoroughly with the KP bioscaffold until complete homogeneity was achieved. The resulting KPSF was treated with methanol to convert the Silk I structure in the SF to Silk II, which is insoluble in water and consists of β-sheet structures; thus, the proteinaceous structures in the composite were tightly packed. Water-insoluble, flexible, and moldable KPSF was then lyophilized to produce the KPSF bioscaffold. When kneaded with water, KP and KPSF bioscaffolds exhibit a ductile-sticky structure, allowing for easy shaping of the desired form. An in-depth investigation was performed into the structural, mechanical, and morphological properties of both lyophilized bioscaffolds, and the results were well-discussed by comparing. Based on our findings, the addition of SF to the KP structure resulted in a relative increase in the porosity and flexibility of the composite KPSF bioscaffold. Both bioscaffolds exhibited pro-angiogenic properties without causing any adverse effects, such as necrosis, during the in ovo CAM assay, suggesting their biocompatibility. Overall, the lyophilized and ductile-sticky forms of both biomaterials obtained can be applied in various defect areas in bone tissue engineering applications. In segmental defects characterized by the absence of a portion of bone tissue and must be structured to meet the primary mechanical strength, both lyophilized bioscaffolds can be considered ideal. Additionally, due to its flexible and robust structure, the KPSF bioscaffold can play an essential role in non-load-bearing bone tissue engineering applications. Given their ductile-sticky form upon kneading with water, it is crucial to assess whether KPSF bioscaffolds can maintain structural stability and durability in a complex physiological environment for effective bone reconstruction. In this context, in vitro biodegradation tests and in vivo CAM analysis results can address these concerns. As a result of the in vitro enzymatic biodegradation test performed by exposing the samples to the enzymatic solution for 10 days at 37 °C under shaking, it was reported that minimal weight changes were observed and maintained their structural integrity, albeit with a slight softening in the aqueous solution. Furthermore, stereomicroscopic images from in ovo CAM analysis show that the implanted materials remained on the CAM surface for four days, demonstrating their stability and structural integrity even in a motile chick embryo. However, it should be noted that the results of this study may not fully simulate real body conditions.

On the other hand, the easily moldable ductile-sticky forms of both materials are more suitable for cavitary defects where only the defect area needs to be filled without providing mechanical support. Due to the plasticizing effect of citric acid used as a crosslinker, KP and KPSF materials have gained a ductile-sticky form. In cavitary bone defects, the ductile-sticky nature of materials offers an advantage in terms of facilitating adhesion and filling the damaged area.

Furthermore, the proposed methods for preparing both biomaterials are easily applicable for incorporating bio-ceramic materials such as hydroxyapatite and resorbable calcium phosphates to enhance osteoinductive properties for further studies in bone tissue engineering applications.

Supporting Information

Supporting Information is available from the Wiley Online Library or from the author.

Acknowledgements

The authors thank the Çanakkale Onsekiz Mart University Scientific Research Projects Coordination Unit (Project ID: FYL-2022-3981) for the financial support and acknowledge the Çanakkale Onsekiz Mart University Science and Technology Application and Research Center (ÇOBILTUM) providing facilities for analysis. The authors also thank Mr. Yücel Okatali (MER-TER Medical, Eskişehir, Türkiye) for the HC staining.

Conflict of Interest

In the study mentioned above, the proposed method regarding keratin extraction from wool is related to a patent application (TPE 2014/02104, Turkish Patent & Trademark Office), which is corresponded by Dr. Yavuz Emre Arslan (Ph.D.) and Dr. Tugba Sezgin Arslan (Ph.D.)

Author Contributions

S.B. performed methodology, formal analysis, investigation, and data curation. T.S.A. performed methodology, formal analysis, data curation, investigation, and wrote the original draft. Y.E.A. performed conceptualization, project administration, investigation, funding acquisition, methodology, supervision and wrote, reviewed, and edited the final manuscript.

Data Availability Statement

The data that support the findings of this study are available from the corresponding author upon reasonable request.

Keywords

bone filler materials, bone tissue engineering, Hydrolyzed wool-keratin, paste, silk fibroin

Received: April 19, 2024
Revised: July 2, 2024
Published online: July 22, 2024

[1] S. Kashte, A. K. Jaiswal, S. Kadam, *Tissue Eng. Regen. Med.* **2017**, *14*, 1.
[2] J. J. Li, M. Ebied, J. Xu, H. Zreiqat, *Adv. Healthc. Mater.* **2018**, *7*, 1701061.
[3] W. Wang, K. W. K. Yeung, *Bioact. Mater.* **2017**, *2*, 224.
[4] E. M. M. Van Lieshout, G. H. Van Kralingen, Y. El-Massoudi, H. Weinans, P. Patka, *BMC Musculoskelet. Disord.* **2011**, *12*, 34.
[5] M. Farokhi, F. Mottaghitalab, S. Samani, M. A. Shokrgozar, S. C. Kundu, R. L. Reis, Y. Fatahi, D. L. Kaplan, *Biotechnol. Adv.* **2018**, *36*, 68.
[6] F. R. Maia, A. R. Bastos, J. M. Oliveira, V. M. Correlo, R. L. Reis, *Bone* **2022**, *154*, 116256.
[7] Y. Esparza, A. Ullah, Y. Boluk, J. Wu, *Mater. Des.* **2017**, *133*, 1.
[8] N. Bloise, A. Patrucco, G. Bruni, G. Montagna, R. Caringella, L. Fassina, C. Tonin, L. Visai, *Materials* **2020**, *13*, 3052.
[9] X. Ding, Y. Huang, X. Li, S. Liu, F. Tian, X. Niu, Z. Chu, D. Chen, H. Liu, Y. Fan, *J. Biomed. Mater. Res. Part A* **2021**, *109*, 515.
[10] L. Gambari, E. Amore, R. Raggio, W. Bonani, M. Barone, G. Lisignoli, B. Grigolo, A. Motta, F. Grassi, *Mater. Sci. Eng. C* **2019**, *102*, 471.
[11] G. Fernandez de Grado, L. Keller, Y. Idoux-Gillet, Q. Wagner, A.-M. Musset, N. Benkirane-Jessel, F. Bornert, D. Offner, *J. Tissue Eng.* **2018**, *9*, 204173141877681.
[12] A. J. Aho, T. Tirri, J. Kukkonen, N. Strandberg, J. Rich, J. Seppälä, A. Yli-Urpo, *J. Mater. Sci. Mater. Med.* **2004**, *15*, 1165.
[13] V. G. Muir, J. A. Burdick, *Chem. Rev.* **2021**, *121*, 10908.
[14] Y. E. Arslan, T. Sezgin Arslan, B. Derkus, E. Emregul, K. C. Emregul, *Colloids Surf., B* **2017**, *154*, 160.
[15] C. Genc, Y. C., H. D., B. Karaca, F. Kiran, Y. E. Arslan, *Int. J. Biol. Macromol.* **2022**, *195*, 492.
[16] F. Cal, T. Sezgin Arslan, B. Derkus, F. Kiran, U. Cengiz, Y. E. Arslan, *ACS Appl. Bio Mater.* **2021**, *4*, 7266.
[17] H. D. Yilmaz, U. Cengiz, Y. E. Arslan, F. Kiran, A. Ceylan, *J. Biosci. Bioeng.* **2021**, *131*, 420.
[18] E. Karakaya, Y. K. Erdogan, T. S. Arslan, Y. E. Arslan, S. Odabas, B. Ercan, E. Emregul, B. Derkus, *Macromol. Biosci.* **2022**, *22*, 1.
[19] M. W. Laschke, K. Witt, T. Pohlemann, M. D. Menger, *J. Biomed. Mater. Res. Part B Appl. Biomater.* **2007**, *82*, 494.
[20] H. H. k. Xu, P. Wang, L. Wang, C. Bao, Q. Chen, M. D. Weir, L. C. Chow, L. Zhao, X. Zhou, M. A. Reynolds, *Bone Res.* **2017**, *5*, 17056.
[21] A. M. Keppler, M. M. Saller, P. Alberton, I. Westphal, F. Heidenau, V. Schönitzer, W. Böcker, C. Kammerlander, M. Schieker, A. Aszodi, C. Neuerburg, *J. Orthop. Surg. Res.* **2020**, *15*, 32727506.
[22] R. C. de Guzman, J. M. Saul, M. D. Ellenburg, M. R. Merrill, H. B. Coan, T. L. Smith, M. E. Van Dyke, *Biomaterials* **2013**, *34*, 1644.
[23] D. N. Rockwood, R. C. Preda, T. Yücel, X. Wang, M. L. Lovett, D. L. Kaplan, *Nat. Protoc.* **2011**, *6*, 1612.
[24] B. Derkus, Y. E. Arslan, A. T. Bayrac, I. Kantarcioglu, K. C. Emregul, E. Emregul, *Sens. Act. B Chem.* **2016**, *228*, 725.
[25] M. Puerta, M. S. Peresin, A. Restrepo-Osorio, *Front. Bioeng. Biotechnol.* **2020**, *8*, https://doi.org/10.3389/fbioe.2020.523949.
[26] A. Samancioglu, B. Aydin, E. Ozudogru, Y. E. Arslan, *Mater. Res. Express* **2023**, *10*, 085401.
[27] M. Isik, E. Karakaya, T. S. Arslan, D. Atila, Y. K. Erdogan, Y. E. Arslan, H. Eskizengin, C. C. Eylem, E. Nemutlu, B. Ercan, M. D'Este, B. O. Okesola, B. Derkus, *Adv. Healthc. Mater.* **2023**, *12*, 2203044.
[28] D. Ribatti, *Reprod. Toxicol.* **2017**, *70*, 97.
[29] E. A. Sokolenko, U. Berchner-Pfannschmidt, S. C. Ting, K. W. Schmid, N. E. Bechrakis, B. Seitz, T. Tsimpaki, M. M. Kraemer, M. Fiorentzis, *Pharmaceutics* **2022**, *14*, 13.
[30] S. D. Aznar-Cervantes, A. Pagan, B. Monteagudo Santesteban, J. L. Cenis, *Sci. Rep.* **2019**, *9*, 6703.
[31] Y.-Q. Zhang, *Bio-Protocol*, https://doi.org/10.21769/BioProtoc.3054.
[32] G. Yildiz, Y. E. Arslan, B. Derkus, B. Sezgin, Y. Z. Menceloglu, G. R. Bayar, *J. Bioact. Compat. Polym.* **2024**, *39*, 46.
[33] H. Y. Wang, Y. Q. Zhang, *Soft Matter* **2013**, *9*, 138.
[34] D. O. S. Ramirez, R. A. Carletto, C. Tonetti, F. T. Giachet, A. Varesano, C. Vineis, *Food Packag. Shelf Life* **2017**, *12*, 100.
[35] B. Ghanbarzadeh, H. Almasi, A. A. Entezami, *Ind. Crops Prod.* **2011**, *33*, 229.
[36] B. Bhandari, S. S. J. Singh, N. M. Rose, *J. Appl. Nat. Sci.* **2018**, *10*, 102.
[37] Y. Tian, Q. Wu, F. Li, Y. Zhou, D. Huang, R. Xie, X. Wang, Z. Zheng, G. Li, *Colloids Surf., B* **2021**, *208*, 112080.
[38] M. Abou Taleb, S. Mowafi, C. Vineis, A. Varesano, D. O. Sanchez Ramirez, C. Tonetti, H. El-Sayed, *J. Nat. Fibers* **2022**, *19*, 3351.
[39] C. Narita, Y. Okahisa, I. Wataoka, K. Yamada, *ACS Omega* **2020**, *5*, 22786.
[40] S. Feroz, N. Muhammad, G. Dias, M. A. Alsaiari, *J. Mol. Liq.* **2022**, *350*, 118595.
[41] K. Song, H. Xu, B. Mu, K. Xie, Y. Yang, *J. Clean. Prod.* **2017**, *150*, 214.
[42] M. Mour, D. Das, T. Winkler, E. Hoenig, G. Mielke, M. M. Morlock, A. F. Schilling, *Materials* **2010**, *3*, 2947.
[43] Y. Tao, S. Liu, *J. Phys. Conf. Ser.* **2023**, *2468*, 012095.
[44] S. Gundu, A. K. Sahi, N. Varshney, J. Varghese, N. K. Vishwakarma, S. K. Mahto, *J. Biomater. Sci., Polym. Ed.* **2022**, *33*, 2220.
[45] N. Abbasi, S. Hamlet, R. M. Love, N. T. Nguyen, *J. Sci. Adv. Mater. Devices* **2020**, *5*, 1.
[46] J. A. Choren, S. M. Heinrich, M. B. Silver-Thorn, *J. Mater. Sci.* **2013**, *48*, 5103.
[47] Y.-T. Jian, Y. Yang, T. Tian, C. Stanford, X.-P. Zhang, K. Zhao, *PLoS One* **2015**, *10*, e0128138.
[48] J. K. Placone, J. Navarro, G. W. Laslo, M. J. Lerman, A. R. Gabard, G. J. Herendeen, E. E. Falco, S. Tomblyn, L. Burnett, J. P. Fisher, *Ann. Biomed. Eng.* **2017**, *45*, 237.
[49] X. Cui, S. Xu, W. Su, Z. Sun, Z. Yi, X. Ma, G. Chen, X. Chen, B. Guo, X. Li, *J. Biomed. Mater. Res. Part B Appl. Biomater.* **2019**, *107*, 1452.
[50] V. P. Ribeiro, A. da Silva Morais, F. R. Maia, R. F. Canadas, J. B. Costa, A. L. Oliveira, J. M. Oliveira, R. L. Reis, *Acta Biomater.* **2018**, *72*, 167.
[51] Z. Luo, Q. Zhang, M. Shi, Y. Zhang, W. Tao, M. Li, *Adv. Mater. Sci. Eng.* https://doi.org/10.1155/2015/315397.

